2-D IRREGULAR SITE RESPONSE CHARACTERISTICS BY BEM-FEM HYBRID ANALYSIS

Hirokazu TAKEMIYA*, Tatsuo TOMONO**,
Masaki ONO*** and Kiyotaka SUDA***

This paper concerns the two-dimensional (2-D) amplification of seismic ground motions by alluvium deposits in view of their configuration. Various hybrid procedures between the boundary element method (BEM) and the finite element method (FEM) are developed for the analysis. The formulation first evaluates the far field impedance by the BEM and then incorporates it into the near field FEM descretization, based on the weighted residual method. The steady state harmonic responses are investigated for the P, SV and Rayleigh wave incidence. The response characteristics are clarified with respect to the dimensionless frequency as defined by the ratio of the surface width and the incident wave length and to the depth of the deposits. Some useful findings from the case studies are pointed out in comparison to the one-dimensional (1-D) analysis.

Keywords: *two dimensional site amplification, topography, inplane wave scattering, BEM–FEM hybrid*

1. INTRODUCTION

Observations of past seismic damage of structures/soils indicate that the surface soft soil amplification for seismic waves might be the primary cause. The vertical shear wave propagation (1-Dimensional : 1-D theory) has been widely employed for evaluating the surface soil motions. However, in view of the surface/subsurface irregularities, the use of a more complete (at least the 2-Dimensional : 2-D) modeling which can characterize a non-flat free surface for a canyon or a non-flat subsurface for an alluvium deposit, is mandatory to better interpret the actual phenomenon. Irregular site configuration, when seismic input motion is specified, generates scattered waves as illustrated in **Fig.1** This leads the amplification/deamplification of the surface response of the near field in comparison to the far field response. At the soft soil deposits significantly amplified response is observed and substantial local surface wave is subsequently generated.

Reviewing past concerned works, we note that the site analysis was started on harmonic antiplane motions for its simplicity[1),2)]. These procedures are classified as follows : the discrete wave number solution method, the direct boundary element method (DBEM), the indirect boundary element method (IDBEM) (source force), and the hybrid method between the BEM for far field and the finite element method (FEM) for near field. These works pointed out the significance of the surface/subsurface effects on the wave scattering

 * Professor, Department of Civil Engineering, Okayama University (Okayama 700)
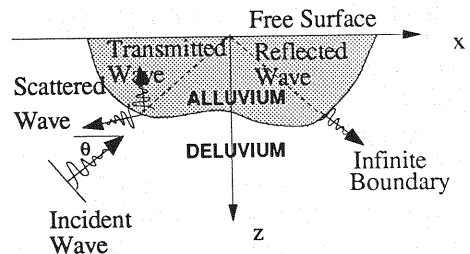 ** Graduate student
 *** CAD Lab., Hazama-Gumi, Ltd.

Fig.1 Wave scattering by alluvium deposits

through the frequency domain analysis. The detailed review is found in Refs. 3 and 4. The investigation for inplane harmonic motions was then addressed ; in this case the wave field is coupled by the P and SV waves. Since the associated displacement potentials derive the decoupled Helmholtz equations, the similar procedure for the SH wave field can be applied to the P/SV wave incidence also. The DBEM which incorporates the Green function for a fullspace was used by Kobayashi[4)] ; the IDBEM with point sources and the associated potential Green functions for a halfspace was adopted by Wong[5)], Sanchez-Sesma, Bravo, and Herrera[6)] and Dravinski and Mossessian[7)] ; Vogt, Wolf and Bachmann[8)] employed uniformly distributed forces. Recently, the hybrid method of FEM and IDBEM has been proposed by Mossessian and Dravinski[9)], Uesugi and Ohtsu[10)], and Khair, Datta and Shah[11)]. Introducing source potentials to interpret scattered waves into the semi-infinity of a halfplane is an effective solution method, but special care should be taken in choosing the source position and the numbers.

In this paper, revised from the authors publication[12)], the scattering of harmonic wave due
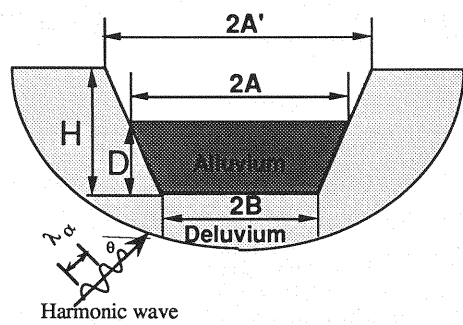
Fig.2　Irregular site model

to topographical boundary is analyzed for various site configurations. Hybrid procedure of the FEM for near field and the BEM for the semi-infinitely extending far field is developed, based on the weighted residual concept to make use of the advantages of the respective method in modeling and analysis. The substructure approach is taken in the formulation; first the far field impedance function is computed and then incorporated into the FEM near field analysis. The comparative approaches are adopted for cross verification among them; one is the DBEM application along the interface between near and far fields, and the other is the IDBEM application which takes certain offset sources as intermediate unknown parameters. Both BEM analyses herein employ the Green function of multilayered elastic medium for concentrated/uniformly distributed load (Takemiya and Arioka[13]), in addition to the Stoke's solution for a full space. The point of investigation is focused on the effect of the 2-D site topography with regard to incident wave types and wave lengths, clarifying the topograpy in which the 1-D analysis can be and cannot be applied to compute the soil amplification. The trapezoidal-shape soil deposits, as illustrated in **Fig.2**, is considered at representative non-dimensional frequencies, as defined by the ratio of the surface width of soil deposit 2A to the incident wave length λ, i.e. $\eta = 2A/\lambda$. For the seismic analysis, various types of incident inplane waves such as SV, P and Rayleigh waves are assumed. The aspect ratio B/D of soil deposit width B to its depth D is varied to compare the 2-D response with the results of 1-D analysis

2. FORMULATION

(1) Superposition of wave fields

The irregular site is split into the surface soil deposits and the surrounding far field. The input seismic motion is prescribed as an incident wave defined at the free field (denoted by superscript f). The non-flat subsurface of soil deposits reflects the incident waves and generates scattered waves

(denoted by superscript s) in the far field. In the near field the wave field is composed of the transmitted waves from the far field and the reflected waves at the free surface. See **Fig.1**. Thus, the total displacement and traction become,

$$u = u^f + u^s, \quad t = t^f + t^s \cdots\cdots\cdots\cdots (1),(2)$$

Far field, presumably comprising uniform or uniformly layered soils, could be modeled and analyzed either by the direct BEM or by the indirect BEM. The near field, on the other hand, indicating nonhomogeneous soils, is modeled by the FEM. The weighted residual technique is employed to advantage to formulate the coupling between the FEM and BEM domains.

(2) BEM for scattered wave field
a) Direct BEM

For the wave scattering in the far field, we get the following boundary integral equation along the subsurface S_b of alluvium deposits.

$$cu^s(x) + \text{p.v.} \int_{S_b} G_t(x,y) u^s(y) ds(y)$$
$$= \int_{S_b} G_u(x,y) t^s(y) ds(y) \cdots\cdots\cdots\cdots (3)$$

in which $G_u(x,y)$ and $G_t(x,y)$ are the Green functions for displacement and traction and u_b^s and t_b^s are the unknown displacement and traction on the interface S_b and c is the so-called free term due to the singularity of function $G_t(x,y)$ at the point of force application. The indication p.v. means that the integral is performed in the sense of the Cauchy's principal value. The procedure to compute the displacement and traction Green function for a layered halfplane is published in Ref.13. in detail.

The boundary S_b is discretized into M elements. The associated displacement and traction are given by use of the interpolation function N_u and N_t, respectively, as

$$u_b^s(y) = N_u(y) \, \widehat{u}_b^s, \quad t_b^s(y) = N_t(y) \, \widehat{t}_b^s \cdots (4),(5)$$

These leads Eq.(3) to

$$H\widehat{u}_b^s = G \, \widehat{t}_b^s \cdots\cdots\cdots\cdots\cdots\cdots\cdots (6)$$

in which the symbol stands for the nodal values. The matrix G and H are computed elementwise whose integral operations in the local coordinate ξ are expressed as

$$G = \sum_{e=1}^{M} \int_{-1}^{1} G_u(\widehat{x}, \xi) N_t(\xi) J(\xi) d\xi \cdots\cdots\cdots\cdots (7)$$

$$H = cI + \sum_{e=1}^{M} \int_{-1}^{1} G_t(\widehat{x}, \xi) N_u(\xi) J(\xi) d\xi \cdots\cdots (8)$$

in which $J(\xi)$ is the Jacobian from the global to local coordinates transformation. Diagonal terms of matrix H for source elements are computed by the static rigid body displacement technique and the subelement division for the numerical Guass

integration. Eq.(6) is modified in terms of the total wave field from Eqs.(1) and (2),

$$H(\widehat{u}_b - \widehat{u}_b^f) = G(\widehat{t}_b - \widehat{t}_b^f) \quad\cdots\cdots\cdots (9)$$

in which the discretized quantities are used for the free field response. The discretized traction on the boundary S_b is then obtained as

$$\widehat{t}_b = (G)^{-1}H(\widehat{u}_b - \widehat{u}_b^f) + \widehat{t}_b^f \cdots\cdots\cdots (10)$$

b) Indirect BEM (Source force method)

We assume that the scattered wave field will be reproduced by imposing fictitious distributed force $p(x)$ appropriately on a surface S_b'. The source location S_b' is offset by a small distance ε from S_b outside to avoid the singularity in the Green function for the above computation. The relevant Green functions for displacement $G_u(y,x)$ and traction $G_t(y,x)$ for point/uniformly distributed forces are those identical with the DBEM. Therefore, the displacement u_p^s and the traction t_p^s at the position y are evaluated as

$$u_p^s(y) = \int_{S_b} G_u(y,x)p(x)ds(x) \cdots\cdots\cdots (11)$$

$$t_p^s(y) = \int_{S_b} G_t(y,x)p(x)ds(x) \cdots\cdots\cdots (12)$$

The unknown force function $p(x)$ is determined as to satisfy the boundary integral equation (3) when Eq.(12) is substituted for the traction. This results in the case when the weighted residual procedure is taken for the traction with the weighting function of $G_u(x,y)$. Since the singularity does not exist in this case, we get in place of Eq.(3)

$$\int_{S_b} G_t(x,y)u^s(y)ds(y)$$
$$= \int_{S_b}\int_{S_b'} G_u(x,y)G_t(y,x')p(x')ds(x')ds(y)$$
$$\cdots\cdots\cdots (13)$$

When S discrete numbers of source forces are used, Eqs.(11) and (12) become

$$u_p^s(y) = \sum_{s=1}^{S} G_u(y,\widehat{x}_s)p_s \cdots\cdots\cdots (14)$$

$$t_p^s(y) = \sum_{s=1}^{S} G_t(y,\widehat{x}_s)p_s \cdots\cdots\cdots (15)$$

so that Eq.(13) is expressed as

$$\int_{S_b} G_t(x,y)u^s(y)ds(y)$$
$$= \int_{S_b}\sum_{s=1}^{S} G_u(x,y)G_t(y,\widehat{x}_s')p_s ds(y) \cdots\cdots (16)$$

The discretized form for Eq.(16) results in

$$H\widehat{u}_b^s = \overline{G}^T P \cdots\cdots\cdots (17)$$

in which

$$\overline{G} = \sum_{e=1}^{M}\sum_{s=1}^{S}\int_{-1}^{1} G_u(\widehat{x},\xi)G_t(\xi,\widehat{x}_s')J(\xi)d\xi \cdots (18)$$

$$H = \sum_{e=1}^{M}\int_{-1}^{1} G_t(\widehat{x},\xi)N_u(\xi)J(\xi)d\xi \cdots\cdots (19)$$

Further, simplification of the integration is made by assuming linear interpolation for the variation of Green functions between adjacent nodal points such that

$$G_u(\widehat{x}_s,\xi) = N_u(\xi)\widehat{G}_u(\widehat{x}_s) \cdots\cdots\cdots (20)$$

$$G_t(\widehat{x}_s,\xi) = N_t(\xi)\widehat{G}_t(\widehat{x}_s) \cdots\cdots\cdots (21)$$

Then, the elementwise integration in Eqs.(18) and (19) are performed analytically, leading Eq.(17) into

$$\widehat{H}\widehat{u}_b^s = \widehat{G}^T P \cdots\cdots\cdots (22)$$

in which

$$\widehat{G} = \sum_{m=1}^{M} \widehat{G}_{tm}{}^T L_m \widehat{G}_{um} \cdots\cdots\cdots (23)$$

$$\widehat{H} = \sum_{m=1}^{M} \widehat{G}_{tm} L_m \cdots\cdots\cdots (24)$$

with

$$L_m = \int_{-1}^{1} N_t(\xi)^T N_u(\xi)J(\xi)d\xi \cdots\cdots\cdots (25)$$

Then, Eq.(22) in terms of the total wave field becomes

$$\widehat{H}(\widehat{u}_b - \widehat{u}_b^f) = \widehat{G}^T P \cdots\cdots\cdots (26)$$

(3) FEM for interior domain

The FEM formulation starts with the virtual work equation in the concerned domain.

$$\int_V \delta\varepsilon^T \sigma du = \int_V \delta u^T(-\rho\omega^2)udv + \int_s \delta u^T p ds$$
$$\cdots\cdots\cdots (27)$$

in which σ=stress, ε=strain, u=displacement, ρ=density, ω=frequency, and $\delta(\ )$'s mean the virtual quantities. The discretization of the domain (with superscript n) leads the governing equation in the partitioned form by the interior degrees of freedom (DOFs) (denoted by subscript i) and the boundary DOFs (denoted by subscript b), as

$$\begin{bmatrix} D_{ii}^n & D_{ib}^n \\ D_{bi}^n & D_{bb}^n \end{bmatrix} \begin{Bmatrix} \widehat{u}_i^n \\ \widehat{u}_b^n \end{Bmatrix} = \begin{Bmatrix} 0 \\ \int_{S_b} N^T t_b^n ds \end{Bmatrix} \cdots\cdots (28)$$

in which $D_s^{n'}$ define the dynamic stiffness matrices of

$$D^n = -\omega^2 M^n + i\omega C^n + K^n \cdots\cdots\cdots (29)$$

with M^n, C^n and K^n denoting, the mass matrix, damping matrix and stiffness matrix, respectively, and i=imaginary unit.

(4) Hybrid approach

The governing equation of the coupled system of the above BEM and FEM domains is made such that the DOFs of the FEM are maintained and the far field impedance function derived from the BEM analysis, which is compatible with the DOFs of the interface boundary, is substituted in the former equation. The weighted residual criteria on displacement and traction is used as follows;

$$\int_b w_d^T(y)(u_{b,\mathrm{BEM}} - u_{b,\mathrm{FEM}})\,ds(y) = 0 \cdots\cdots (30)$$

$$\int_{S_b} w_t^T(y)(t_{b,\mathrm{BEM}} + t_{b,\mathrm{FEM}})\,ds(y) = 0 \cdots\cdots (31)$$

in which $w_d(y)$ and $w_t(y)$ define the independent weighting functions. For displacement and traction, the choice are made as follows :

$$w_d(y) = t_b^s(y) \text{ and } w_t(y) = u_b(y) \cdots (32),(33)$$

a) For the direct BEM approach, Eq.(30) is automatically satisfied so that Eq.(31) is only taken into account. This converts the BEM traction into the FEM nodal forces.

$$L^T(t_b^f + t_b^s) = P_b^n \cdots\cdots\cdots\cdots\cdots (34)$$

in which L is already defined in Eq.(25) elementwise. The impedance matrix for the far field and the associated effective input are then defined as

$$K_{bb}^* = LG^{-1}H, \quad \widehat{p}_b^{*f} = K_{bb}^* \widehat{u}_b^f - L\,\widehat{t}_b^f \cdots (35),(36)$$

Hence, the total governing equation is obtained.

$$\begin{bmatrix} D_{ii}^n & D_{ib}^n \\ D_{bi}^n & D_{bb}^n + K_{bb}^* \end{bmatrix} \begin{Bmatrix} \widehat{u}_i^n \\ \widehat{u}_b^n \end{Bmatrix} = \begin{Bmatrix} p_i^n \\ \widehat{p}_b^{*f} \end{Bmatrix} \cdots\cdots\cdots (37)$$

b) For the indirect BEM approach, after discretization, Eqs.(30) and (31) result in

$$\overline{G}^T P + H(u_b^f - \widehat{u}_b) = 0, \quad H^T P + P_b^f + P_b^n = 0$$
$$\cdots\cdots\cdots\cdots\cdots (38),(39)$$

Eliminating the unknown forces P from Eqs.(38) and (39) derives the far field impedance K_{bb}^* and the input forces $\widehat{P}_b^{*f}$ to the FEM domain. Hence, the total governing equation results.

$$\begin{bmatrix} D_{ii}^n & D_{ib}^n \\ D_{bi}^n & D_{bb}^n + K_{bb}^* \end{bmatrix} \begin{Bmatrix} \widehat{u}_i^n \\ \widehat{u}_b^n \end{Bmatrix} = \begin{Bmatrix} \widehat{P}_i^n \\ \widehat{P}_b^{*f} \end{Bmatrix} \cdots\cdots\cdots (40)$$

with

$$K_{bb}^* = H^T(\overline{G}^T)^{-1}H, \quad \widehat{P}_b^{*f} = K_{bb}^* \widehat{u}_b^f - \widehat{P}_b^f$$
$$\cdots\cdots\cdots\cdots\cdots (41),(42)$$

3. NUMERICAL ANALYSIS AND DISCUSSION

Validity of the present hybrid method is first studied both for the DBEM and the IDBEM by comparing the results with the pubilshed ones for a half-circular soil deposit and for a half-circular canyon for various incident waves. For such a simple model, the fundamental solution for a full plane (Stoke's solution) and the Green function for a uniform halfplane are available. The relevant analytical expression for an elastic halfplane motion for the far filed response are referred to standard text books. However, aiming at the further development to the multilayered soils, the present method makes the formulation amenable to them. Since the wave propagation matrix
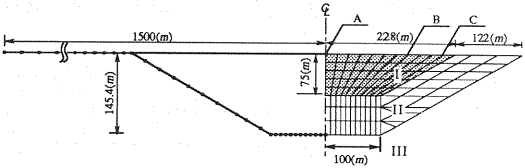

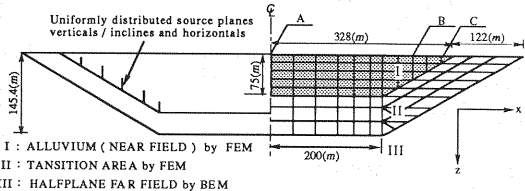**Fig.3.a** Model for numerical computation, Case 1 ; DBEM and FEM

Fig.3.b Model for numerical computation, Case 2 ; IDBEM and FEM

I : ALLUVIUM (NEAR FIELD) by FEM
II : TANSITION AREA by FEM
III : HALFPLANE FAR FIELD by BEM

Table 1 Soil Properties

	Shear velocity	Density	Damping ratio	Poisson ratio
Alluvium Deposit	200 m/s	1.6 t/m³	0.10	0.45
Far Field	500 m/s	2.0 t/m³	0.02	0.35

involves the exponential functions which may diverge for a long distance in depth between force and observation points, an additional automatic subdivision process for the original layers are implemented. The details are referred to the Ref.12. The free field surface responses of layers are computed by the Haskell method[14].

In what follows, a parametric study is conducted for the layered soil deposits of trapezoidal configuration. The dimensions and the soil properties are indicated in **Fig.3** and **Table 1**. Two aspect ratios $B/H = 1.3$ and 2.7 between width B and depth H are considered. Incident waves are assumed as the P, SV body waves of various angles of incidence, and the Rayleigh surface wave. The horizontal propagation is taken toward the positive x-direction (from let to right in **Fig. 3**). The Rayleigh wave has a long period and propagating nature in horizontal direction, which are worried to have give a substantial effect upon the displacement sensitive extended structures. The main parameter which can describe the behavior of the soil deposits is the following dimensionless frequency.

$$\eta = 2A/\lambda_{SV} = (2A/V_s)f \text{ or } \eta = 2A/\lambda_p = (2A/V_p)f$$
$$\cdots\cdots\cdots\cdots\cdots\cdots (43)$$

in which $2A$ is the surface width of soil deposits, λ_{SV} is the S-wave length, λ_p is the P-wave length for the far field halfplane, and f is the frequency concerned.
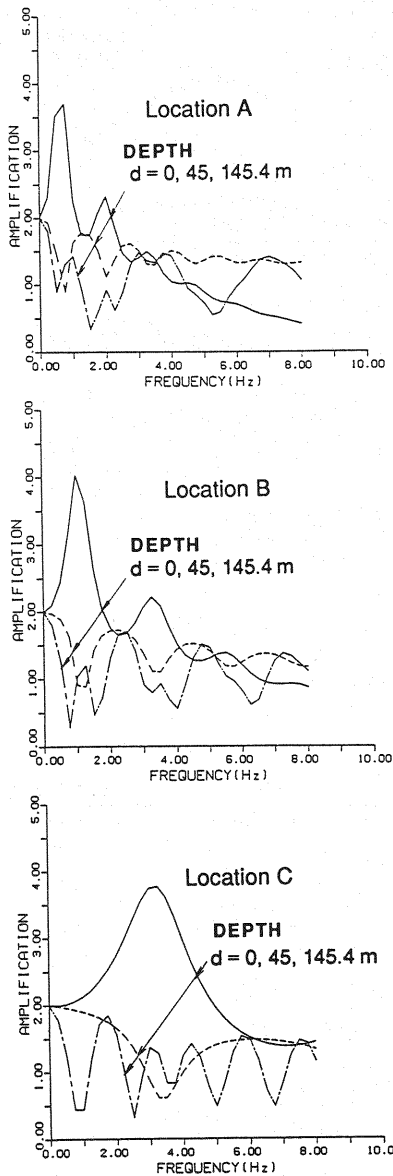
The 1-D model which is composed of the soil

Fig.4 Resonance curves from 1-D analysis

fication for the Case 1 in which the response is presented in a normalized form by the far field surface response. In applying the IDBEM to evaluate the far field impedance, investigation is first made on determining of the fictitious source planes. Fictitious sources are suggested to have an offset from the actual boundary by around 1/6 of the wave length concerned (Takemiya and Arioka[12]). Two alternative choices are depicted in **Fig.3**. b ; one is a continuous offset planes all along parallel to the interface S_b (legend "inclines and horizontals" as indicated by ✕✕◇), and the other is a number of vertical and norizontal discrete planes along the same interface ("verticals and horizontals" as indicated by —, ⋯). The preliminary IDBEM analyses by use of these different sources yield an excellent matching for the surface response as shown in **Figs.5**.a and **6**.a. As already mentioned in the above Ref. 12, the latter type sources are less time consuming for the Green function computation, consequently for the far field impedance computation. In the present hybrid analysis, note that the FEM modeling is taken to cover the alluvium soil deposit and its neighboring zone from the far field as a transition area from near to far field. This treatment works for improving the solution accuracy when the soil stiffness changes drastically between them. Linear isoparametric elements are used in discretizing both the BEM and FEM domains. Note that the computation accuracy between the DBEM and the IDBEM is quite well for frequency range up to $\eta = 3$ for the SV wave and the Rayleigh wave incidence ; and up to $\eta = 2$ for the P wave incidence. This may be interpreted from the fact that the actual frequency $\omega = 2\pi f$ for the P wave is about two times larger than that for the SV wave when the nondimensional frequency η is kept constant. If the more deliberate consideration is paid to the source numbers and their location, the better matching will be expected between the IDBEM and the DBEM even for the higher values of η. However, as far as our interest lies in extended structures on alluvium deposits, the dimensionless frequency may be confined, for instance, as $\eta < 2$, since this value in view of Eq.(43) corresponds the period longer than 0.7 seconds, which is very plausible in reality.

From the site analysis for $D/H = 1$ (**Figs. 5** though 7), it is clear that the surface response varies significantly by the type of incident wave and by the angle of incidence. The effect of the dimensionless frequency is also remarkable. For the vertical SV wave incidence at low dimensionless frequency, the response mode with only one peak results at the surface center of soil deposits which is about two times greater value than the far
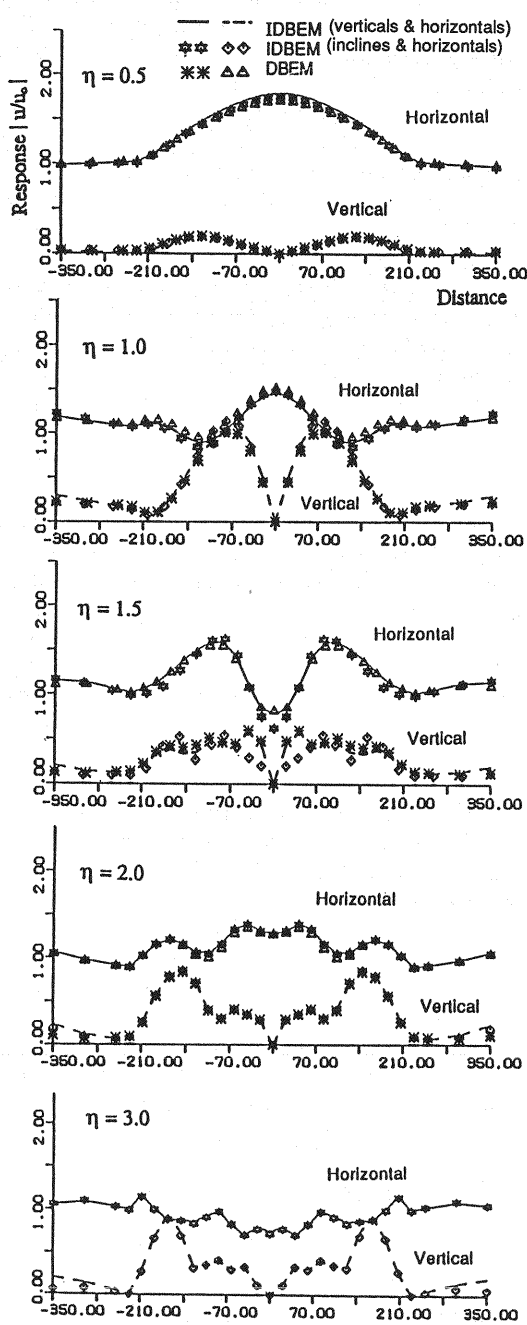
column taken out from the five focus locations in the 2-D soils and assumes fictitiously the horizontal layering in depth is investigated to get the first insight of the global behavior of the soil deposits. **Fig.4** is the results of surface resonance curves at locations of the horizontal distance $x=0$, 60, 100 m for the model case 1 ; $x=0$, 120, 200 m for the model case 2 from the center, where the depth of the surface layer corresponds $d=0$, 45, 145.4 m, respectively. In view of the fundamental frequency f_1 the value of η is assumed in the range of 0.5 through 3 for the 2-dimensional analysis.

Figs.5 through 7 show the 2-D surface ampli-

Fig.5.a Surface response ; SV wave incidence, Angle of incidence $\pi/2$ (Verical)

Fig.5.b Surface response ; SV wave incidence, Angle of incidence $\pi/3$ from horizontal

field surface response, while at high dimensionless frequency the response mode with multiple peaks appears, giving the greater values at the soil deposits ends than the far field surface response. Substantial vertical response component is induced over inclined base as the frequency increases, say η
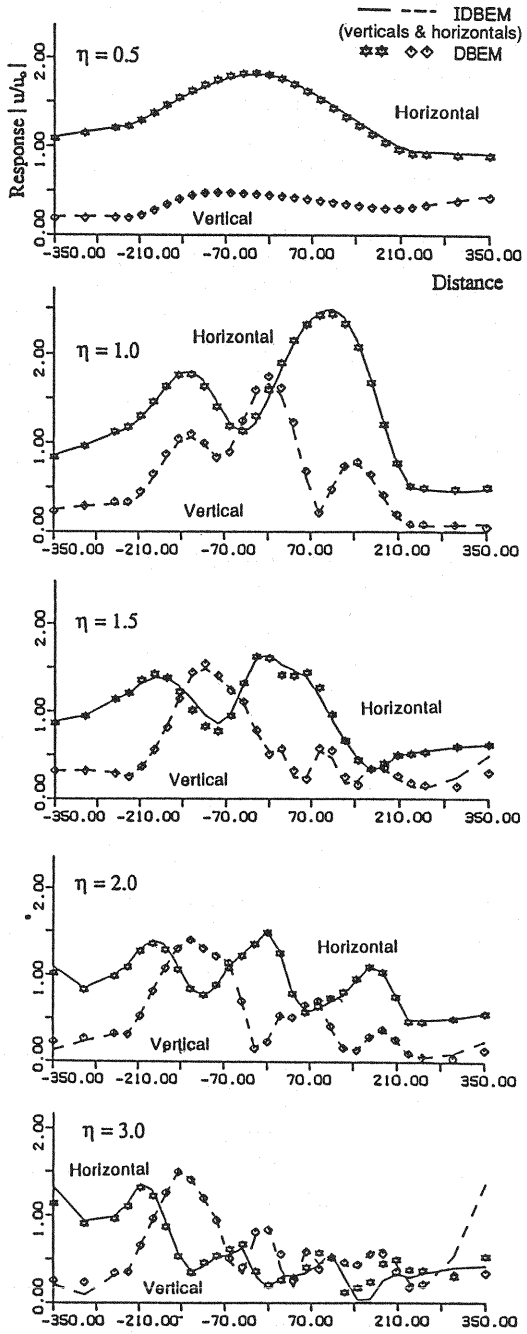
>1. The effect of incident angle also increases the response at the surface over the inclined base ; at η $=1$ more than two times greater value of the far field response results. The same tendency can be observed for the P wave incidence. The Rayleigh wave incidence yields different amplification from
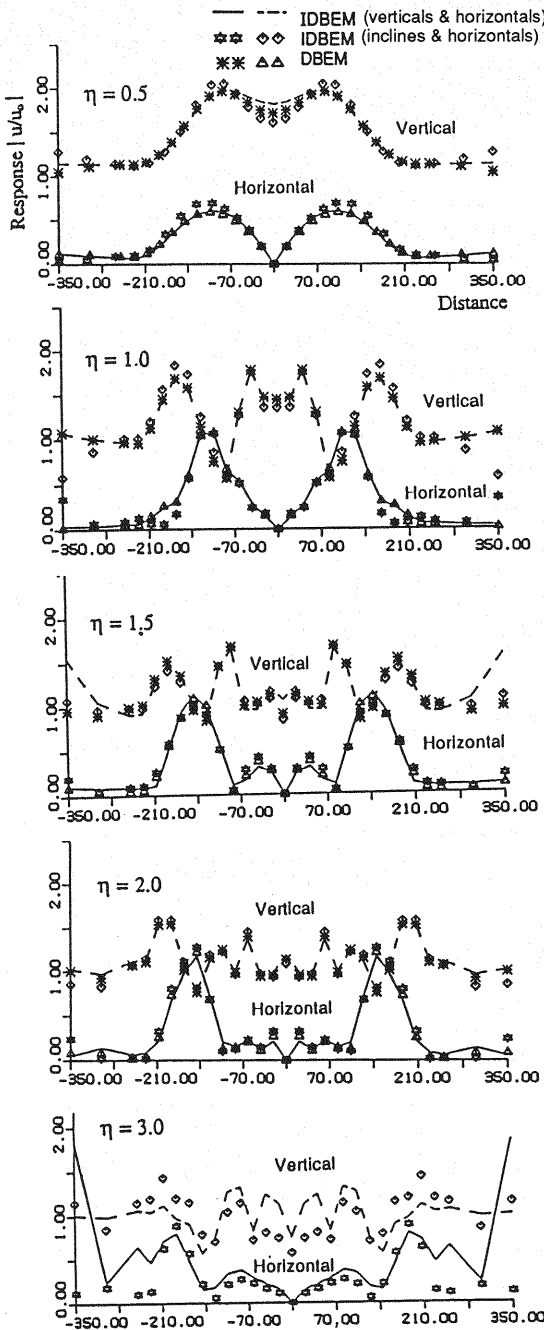
Fig.6.a   Surface response ; P wave incidence, Angle of incidence $\pi/2$ (Verical)
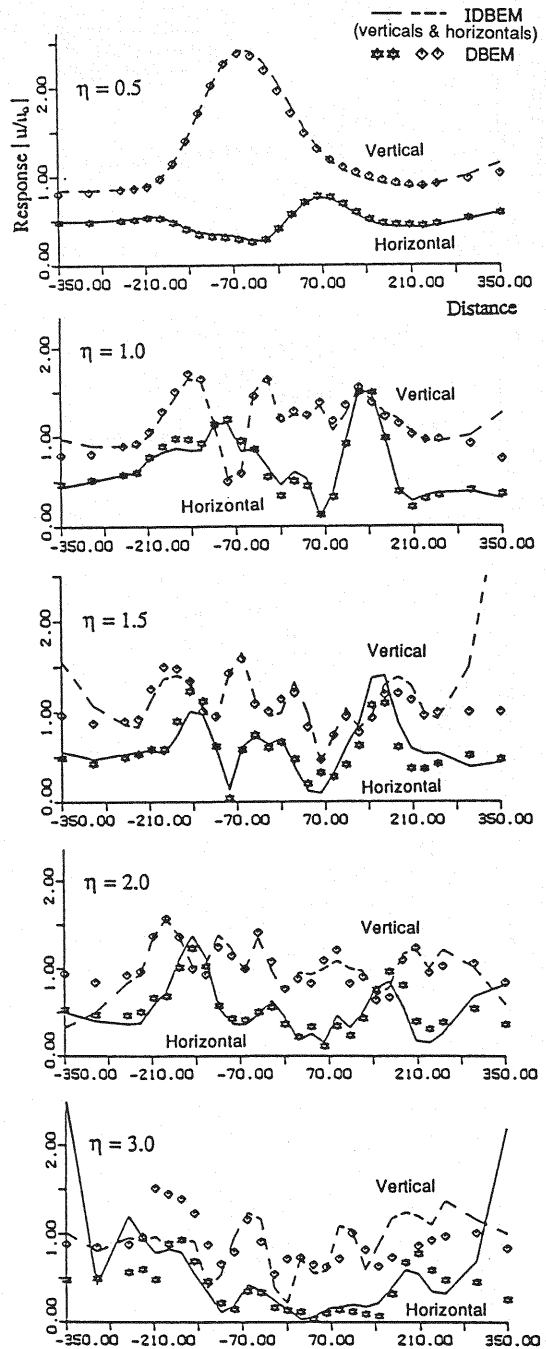
Fig.6.b   Surface response ; P wave incidence, Angle of incidence $\pi/3$ from horizontal

the oblique SV wave incidence, although both are assumede propagate toward the same direction. Note that the wave velocity of the former depends on the frequency. Therefore, the response for the Rayleigh wave may not be readily interpreted equivalently by that for an oblique SV wave

incidence.

In order to clarify the 2-dimensional effect on the behavior of soil deposits, the comparison is made between the 2-D and 1-D analyses for the vertical shear wave incidence. **Figs.**8 and 9 show the responses along depth for the aspect ratios B/D
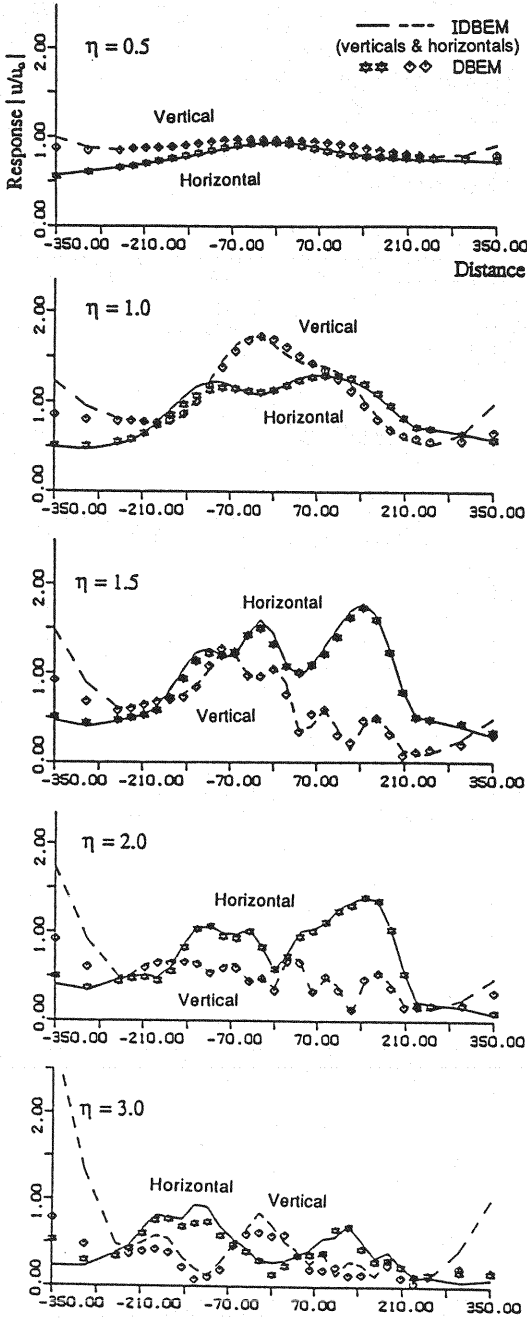
Fig.7 Surface response ; Rayleigh wave incidence

Fig.8 Vertical response profiles ; Case 1, B/D=1.3
─Horizontal (2D Analysis) ; ⋯ Vertical (2D Analysis) ; ✱✱✱ (1D Analysis)

Fig.9 Vertical response profiles ; Case 2, B/D=2.7
─Horizontal (2D Analysis) ; ⋯ Vertical (2D Analysis) ; ✱✱✱ (1D Analysis)

= 1.3, 2.7 at representative dimensionless frequencies. In these figures, the horizontal components should be compared each other while the vertical components are depicted to understand such generation due to the inclined side boundary. When we pay attention to the behavior of soil deposits, the fundamental natural period is of special importance. The 1-D analysis seems to
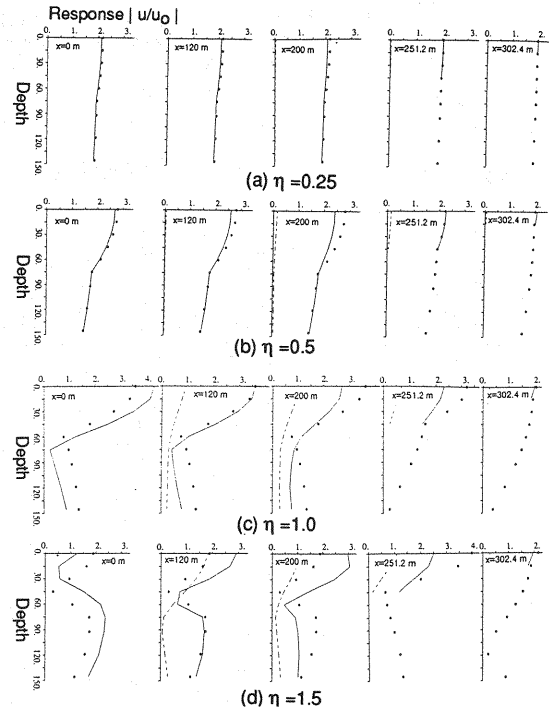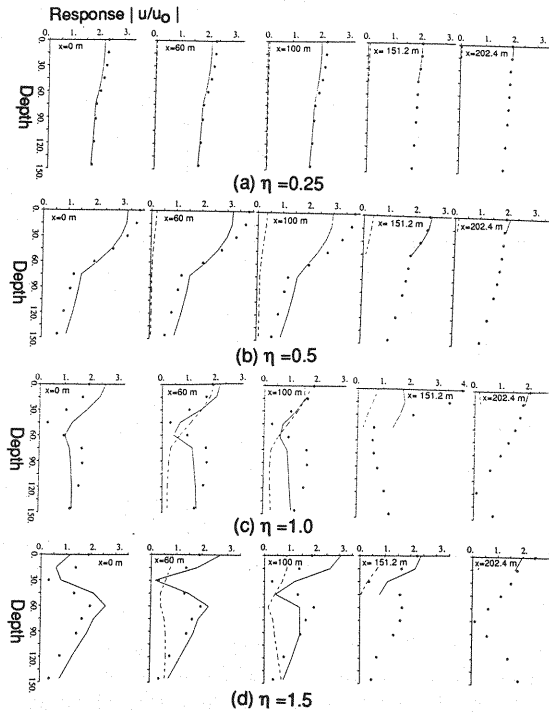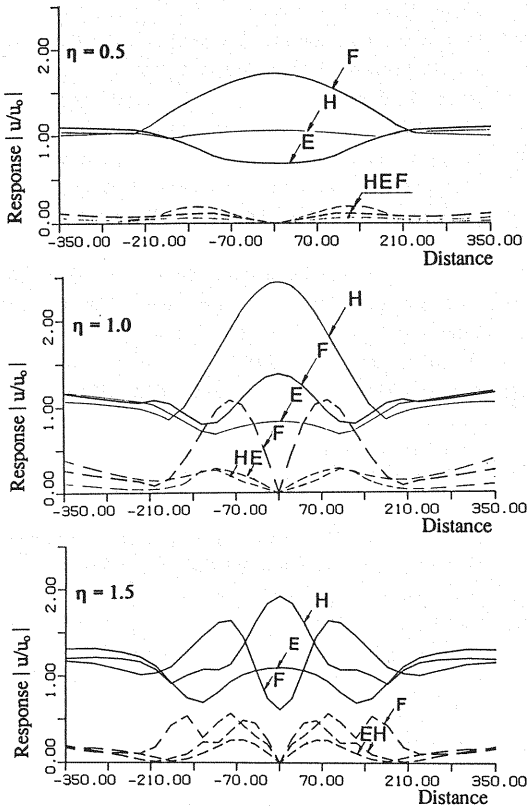
Fig.10 Subsurface depth effect of surface response E; $D/H=0$; H; $D/H=1/2$; F; $D/H=1$,

yield an adequate evaluation only near the surface center for both models considered. At other locations the presence of the inclined subsurface leads the more different response profiles from the 1-D solutions for the aspect ratio $B/D = 1.3$ than for the ratio $B/D = 2.7$ except at very low frequency. At the locations whose horizontal distance $B/D > 3$ roughly, the 1-D analysis seems to be valid for evaluating the response near at the predominant frequency f_1.

Fig.10 indicates the effect of the alluvium deposits depth on the surface amplification for the Case 1. Significant differences are observed according to the parameter D/H; in the figure the legend E, H and F correspond, respectively, to $D/H=0$, 1/2 and 1. The subsurface topography tends to increase the surface response over the flat base in the higher frequency range above f_1 while decreases it below f_1. The fact that the highest peak is attained at a different frequency for different topography may be interpreted by the resonance frequency of the surface alluvium deposit and also by the drastic change of the response mode.

4. CONCLUSION

Various hybrid procedures between the boundary element method (BEM) and the finite element method (FEM) are developed for the 2-dimensional seismic analysis of a trapezoidal alluvium. The indirect and the direct BEM approaches give an excellent matching for the surface response evaluation in the range of the dimensionless frequency (the ratio between the surface width of the alluvium and the incident wave length) which is important for the design of extended structures. The advantage of the indirect BEM with use of vertical and horizontal uniform source forces is noted. From the parametric study, the site amplification, which is normalized by the far field response and indicated as the difference from the 1-D response analysis of the concerned soil column model, is clarified with respect to the incident wave type, the angle of incidence and the dimensionless frequency.

The findings from the parametric study for the dimensionless frequency in the range $0.5 < \eta < 3$ are summarized as follows :

(1) For small dimensionless frequency, the response in the direction of the incident wave force is predominant, giving predominant peak depending on the angle of wave incidence.

(2) For high dimensionless frequency, not only the response along the incident wave force but also the substantial perpendicular response comes out. The vertical wave incidence yields such significant perpendicular respnse at the surface over inclined base. The oblique wave incidence results in the complex response feature, depending on the incident wave type.

(3) The Rayleigh wave incidence yields the comparable vertical and horizontal response components for the dimensionless frequency considered. The similar trend is also observed for the oblique SV wave incidence for high dimensionless frequency. However, the former may not equivalently substitued for the latter since the wave velocity is frequency- dependent in the latter situation.

(4) The depth D of the soil deposit changes the response features tremendously, which must be interpreted by the 2-dimensional vibration modes of soil deposits. However, when the attention is paid to the soil response away from the edge of the soil deposit by the horizontal distance x to satisfy $x/D > 3$, it may properly be evaluated by the 1-dimensional computation.

REFERENCES

1) Trifunac, M.D. : Scattering of Plane SH Waves by a

2D IRREGULAR SITE RESPONSE CHARACTERISTICS
BY BEM-FEM HYBRID ANALYSIS/ *TAKEMIYA · TOMONO · ONO · SUDA*

Semicylindrical Canyon, Earthquake Eng.&Struc. Dyn,. Vol. 1, pp.267~281, 1973.

2) Dravinski, M. : Scattering of SH Waves by Subsurface Topography, J. Eng. Mech. Div., ASCE, Vol.108, No.EM1, pp.1~7, 1982.

3) Bravo, M.A., F.J. Sanchez-Sesma and F.J. Chavez-Garcia : Ground motion on stratified alluvial deposits for incident SH waves, Bull. Seis. Soc. Amer., 78.2, 436~450, 1988.

4) Kobayashi, S. : Some Problems of the Boundary Integral Equation Method in Elastodynamics, Proc. 5th Int. Conf. on Boundary Elements, pp.775~784, 1983.

5) Wong, H.L. : Effect of Surface Topography on The Diffraction of P, SV, and Rayleigh Waves, Bull. Seis. Soc. Amer., 72, pp.1167~1183, 1982.

6) Sanchez-Sesma, F.J., M.A. Bravo, and I. Herrera : Surface Motion of Topographical Irregularities for Incident P, SV, and Rayleigh Waves, Bull. Seis. Soc. Amer., 75, pp.263~269, 1985.

7) Dravinski, M. and T.K., Mossessian : Scattering of Plane Harmonic P, SV, and Rayleigh Waves by Dipping Layers of Arbitrary Shape, Bull. Seism. Soc. Amer., Vol. 77, No.1, pp.212~235, 1987.

8) Vogt, R.F., Wolf, J.P. and H., Bachmann : Wave Scattering by a Canyon of Arbitrary Shape in a Layered Half-space, Earthq. Eng. and Struct. Dyn., Vol.16, pp.803 ~812, 1988.

9) Mossessian, T.K. and M., Dravinski : Application of a Hybrid Method for Scattering of P, SV, and Rayleigh Waves by Near-surface irregularities : Bull. Seis. Soc. Amer., 77, pp.1784~1803, 1987.

10) Uesugi, S. and M., Ohtsu : BEM-FEM Coupling Analysis of The Two-Dimensional Elastic Wave Field in Steady State, Proc. JSCE, No.398/I-10, pp.295~301, 1988. 10.

11) Khair, K.R., S.K., Datta and A.H., Shah, : Amplification of Obliquely Incident Seismic Waves by Cylindrical Alluvial Valleys of Arbitrary Cross-sectional Shape. Part I. Incident P and SV Waves, Bull. Seism. Soc. Amer. Vol. 79, No.3, pp.610~630, 1989.

12) Takemiya, H., M., Ono and K., Suda : BEM-FEM Hybrid Analysis for Topographical Site Response Characteristics, Proc. 2nd Int. Conf. Recent Advances in Eartq. Eng. Soil Dyn. St. Louis, Missouri, USA, 1991. 3.

13) Takemiya, H. and K., Arioka, : Numerical Computation Method of 2D-Green Function of Viscoelastic Layered Halfspace for Concentrated/Distributed Forces, Proc. JSCE, No.441/I-18, pp.57~66, 12.

14) Haskell, N.A. : The Dispersion of Surface Waves of Multi-layered Medai, Bull. Seism. Soc. Amer., Vol. 43, No.1, pp.17~34, 1987.